Metabolomics reveals an essential role for peroxisome proliferator-activated receptor α in bile acid homeostasis[s]

Fei Li,* Andrew D. Patterson,*[,†,§] Kristopher W. Krausz,* Naoki Tanaka,*
and Frank J. Gonzalez[1,]*

Laboratory of Metabolism,* Center for Cancer Research, National Cancer Institute, National Institutes of Health, Bethesda, MD; and Department of Veterinary and Biomedical Sciences[†] and Center for Molecular Toxicology and Carcinogenesis,[§] Pennsylvania State University, University Park, PA

Abstract Peroxisome proliferator-activated receptor α (PPARα) is a nuclear receptor that regulates fatty acid transport and metabolism. Previous studies revealed that PPARα can affect bile acid metabolism; however, the mechanism by which PPARα regulates bile acid homeostasis is not understood. In this study, an ultraperformance liquid chromatography coupled with electrospray ionization quadrupole time-of-flight mass spectrometry (UPLC-ESI-QTOFMS)-based metabolomics approach was used to profile metabolites in urine, serum, and bile of wild-type and *Ppara*-null mice following cholic acid (CA) dietary challenge. Metabolomic analysis showed that the levels of several serum bile acids, such as CA (25-fold) and taurocholic acid (16-fold), were significantly increased in CA-treated *Ppara*-null mice compared with CA-treated wild-type mice. Phospholipid homeostasis, as revealed by decreased serum lysophosphatidylcholine (LPC) 16:0 (1.6-fold) and LPC 18:0 (1.6-fold), and corticosterone metabolism noted by increased urinary excretion of 11β-hydroxy-3,20-dioxopregn-4-en-21-oic acid (20-fold) and 11β,20α-dihydroxy-3-oxo-pregn-4-en-21-oic acid (3.6-fold), were disrupted in CA-treated *Ppara*-null mice. The hepatic levels of mRNA encoding transporters Abcb11, Abcb4, Abca1, Abcg5, and Abcg8 were diminished in *Ppara*-null mice, leading to the accumulation of bile acids in the liver during the CA challenge.ⓘⓡ These observations revealed that PPARα is an essential regulator of bile acid biosynthesis, transport, and secretion.—Li, F., A. D. Patterson, K. W. Krausz, N. Tanaka, and F. J. Gonzalez. **Metabolomics reveals an essential role for peroxisome proliferator-activated receptor α in bile acid homeostasis.** *J. Lipid Res.* 2012. **53:** 1625–1635.

Supplementary key words PPARα • bile acid metabolism • phospholipid metabolism • cholesterol and corticosterone metabolism

Peroxisome proliferator-activated receptor α (PPARα) is a nuclear hormone receptor regulating genes involved in lipid homeostasis, including fatty acid transport and catabolism, lipoprotein metabolism, glucose homeostasis, and inflammation (1, 2). Recent studies have suggested a role for PPARα in bile acid biosynthesis. A previous study reported that the expression level of cholesterol 7α-hydroxylase (Cyp7a1) and 8β-hydroxylase (Cyp8b1) was upregulated in wild-type mice during [4-chloro-6-(2,3-xylidino)-2-pyrimidinylthio] acetic acid (Wy-14,643) treatment and fasting conditions; this effect was diminished in *Ppara*-null mice, thus revealing the involvement of PPARα (3). Another study found that both human *CYP7A1* and mouse *Cyp7a1* promoters were stimulated by fatty acids and Wy-14,643 treatment (4). These studies provided compelling evidence that PPARα can positively regulate bile acid biosynthesis. In contrast to the above observations, it

---

was reported that 0.5% bezafibrate treatment leads to a decrease in liver bile acid and Cyp7a1 expression in wild-type mice and *Ppara*-null mice (5). Others found that Cyp7a1 and cholesterol 27α-hydroxylase (Cyp27a1) were decreased in wild-type mice by ciprofibrate treatment but not in *Ppara*-null mice (6). These results indicate that the activation of PPARα by fibrates can inhibit bile acid biosynthesis; however, bezafibrate and ciprofibrate show different effects on bile acid biosynthesis enzymes in *Ppara*-null mice. Thus, the mechanism by which PPARα controls bile acid homeostasis remains uncertain. Additionally, limited studies revealed that PPARα exert its effect on the bile acid conjugation and transport in the liver and intestine (7, 8).

Recent studies have demonstrated the power of mass spectrometry-based metabolomics to profile metabolic pathways to reveal the mechanism of action of nuclear receptors and the metabolic fate of drugs (9–12). Metabolomics has revealed the downregulated tryptophan-nicotinamide pathways following Wy-14,643 treatment (9) and the decreased excretion of carnitine-conjugated metabolites by fenofibrate treatment in humans (13). Furthermore, an increase in the excretion of glycine conjugated metabolites was observed in *Ppara*-null mice (9), and the long-chain fatty acid carnitines, including palmitoylcarnitine, myristolcarnitine, oleoylcarnitine, and palmitoleoylcarnitine, were elevated in the serum after suppression of PPARα signal transduction by acetaminophen (14).

In the present study, cholic acid (CA)-treated wild-type and *Ppara*-null mice were used to evaluate the functional role of PPARα in bile acid homeostasis. Metabolomics analysis showed that severe liver dysfunction in *Ppara*-null mice was induced during CA challenge, including the disruption of bile acids, phospholipids, and cholesterol homeostasis. Additionally, the excretion of several endogenous cationic and anionic metabolites was significantly affected. Further results demonstrated that PPARα exerted a role in bile acid homeostasis via regulation of bile acid biosynthesis, transport, and secretion.

MATERIALS AND METHODS

Chemicals and reagents

Cholic acid (CA), taurocholic acid (TCA), chenodeoxycholic acid (CDCA), tauro-α/β-muricholic acid (T-α/β-MCA), taurochenodeoxycholic acid (TCDCA), taurodeoxycholic acid (TDCA), tauroursodeoxycholic acid (TUDCA), tauromurideoxycholic acid (TMDCA), chlorpropamide, creatinine, creatine, nicotimamide 1-oxide, xanthurenic acid, and phenylacetylglycine were purchased from Sigma (St. Louis, MO). 11β-Hydroxy-3,20-dioxopregn-4-en-21-oic acid (HDOPA) and 11β,20α-dihydroxy-3-oxo-pregn-4-en-21-oic acid (DHOPA) were ordered from Anbilaunch Consulting (San Meteo, CA). 1-Palmitoyl-*sn*-glycero-3-phosphocholine (LPC 16:0) and 1-stearoyl-*sn*-glycero-3-phosphocholine (LPC 18:0) were obtained from Avanti Polar Lipids, Inc. (Alabaster, AL). All solvents and organic reagents were of the highest obtainable grade.

Animal study

Ppara-null mice and wild-type mice on a C57BL/6N genetic background were maintained under a standard 12 h light/12 h dark cycle with water and a normal diet (NIH-31) provided ad libitum. Handling was in accordance with an animal study protocol approved by the National Cancer Institute Animal Care and Use Committee. Groups of 8- to 12-week-old male mice were put on a synthetic purified diet (AIN-93G, Bio-Serv, NJ) for 5 days before experiment. *Ppara*-null mice and wild-type mice were fed with CA diet (AIN-93G supplemented with 1% CA) and control diet (AIN-93G) for 12 days based on previous studies (15–17). Urine samples were collected and food intake was measured from mice placed individually in metabowls (Jencons, Leighton Buzzard, UK) for 24 h, before treatment, and on days 1, 3, 6, 9, and 12 following the treatment. The mice had ad libitum access to diet and water in these metabolic chambers. All urine samples were stored at −80°C until analyzed. The serum, bile, liver, and kidney tissue were harvested and frozen at −80°C for further analysis at the end of the study.

UPLC-ESI-QTOFMS analysis

Samples for injection were prepared by diluting 20 µl urine with 180 µl 50% aqueous acetonitrile. Serum samples were prepared by 10 µl serum mixed with 190 µl 67% aqueous acetonitrile, and bile samples were prepared by 1 µl bile mixed with 1,000 µl 67% aqueous acetonitrile. The samples were vortexed for 5 min in shaker and centrifuged at 14,000 rpm for 20 min at 4°C to remove particulates and precipitate protein. The supernatant was transferred to an autosampler vial for analysis. A 5 µl aliquot of supernatant samples was injected into the system of ultraperformance liquid chromatography coupled quadrupole time-of-flight mass spectroscopy (UPLC-ESI-QTOFMS). The liquid chromatography system was ACQUITY UPLC® equipment (Waters) consisting of a reverse-phase 2.1 × 50 mm ACQUITY UPLC® BEH C18 1.7 µm column (Waters Corp., Milford, MA) with a gradient mobile phase comprising 0.1% formic acid solution (A) and acetonitrile containing 0.1% formic acid solution (B). The gradient was maintained at 100% A for 0.5 min, increased to 100% B over the next 7.5 min, and returned to 100% A in last 2 min. Data were collected in positive mode and negative mode on a Waters Q-TOF, which was operated in full-scan mode at m/z 100 to 1,000. Nitrogen was used as both cone gas (50 l/h) and desolvation gas (600 l/h). Source temperature and desolvation temperature were set at 120°C and 350°C, respectively. The capillary voltage and cone voltage were 3,000 and 20 V, respectively. Chlorpropamide (5 µM) was added in the sample as the internal standard.

Data processing and multivariate data analysis

Raw data from UPLC-ESI-QTOFMS system were processed using MarkerLynx software (Waters) to generate a data matrix consisting of peak areas corresponding to a unique m/z and retention time (RT) without normalization. After the generation of a multivariated data matrix, this data set was exported into SIMCA-P+12.0 (Umetrics, Kinnelon, NJ) for principal component analysis (PCA). The loadings scatter plots and the contribution lists were used to determine the candidate biomarkers in CA-fed *Ppara*-null mice compared with other group mice.

Identification and quantitation of urinary and serum metabolites

To identify the structure of high-contribution score metabolites, metabolomics databases (Madison Metabolomics Consortium Database and METLIN) were searched to find potential candidates. Seven Golden Rules (18) were used to calculate the mass error based on the elemental compositions of each metabolite. To confirm the identities of markers, authentic standards at 5 to 20 µM in 50% acetonitrile were compared with the urine and serum sample on the condition of MS/MS fragmentation with collision energy ramping from 15 to 35 V. Identities of the

ions were further confirmed by comparison of fragmentation pattern and retention time with authentic compounds.

Quantitation of metabolites in urine and serum was performed using an ACQUITY UPLC system coupled with a XEVO triple-quadrupole tandem mass spectrometer (Waters). The detection and quantitation of biomarkers were accomplished by multiple reaction monitoring (MRM) mass spectrometry. The following MRM transitions were monitored for each metabolite: xanthurenic acid (206→156; ESI$^+$), nicotinamide 1-oxide (139→106; ESI$^+$), phenylacetylglycine (192→74; ESI$^-$), HDOPA (361→121; ESI$^-$), DHOPA (363→121; ESI$^-$), creatinine (114→86; ESI$^+$), creatine (132→90; ESI$^+$), CA (407→343; ESI$^-$), TCA (514→80; ESI$^-$), LPC 16:0 (496→104; ESI$^+$), and LPC 18:0 (524→104; ESI$^+$). The concentrations of metabolites in urine and serum were determined by use of calibration curves constructed with authentic standards. To obtain the accurate concentration of metabolites, 0.5 μM chlorpropamide (277→111; ESI$^+$) was used as the internal standard.

Gene expression analysis

Total RNA was extracted from approximately 100 mg portions of frozen liver and kidney using TRIzol reagent (Invitrogen, Carlsbad, CA). Quantitative real-time PCR (qPCR) was carried out using SYBR green PCR master mix (Superarray) in an ABI Prism 7900HT sequence detection system (Applied Biosystems). QPCR primer sequences are shown in the supplementary Table I. Measured mRNA levels were normalized to those of β-actin (liver) or 18S (kidney) rRNA and expressed as fold change relative to those of wild-type mice fed a control diet.

Serum chemistry

Serum alanine aminotransferase transaminase (ALT), alkaline phosphatase (ALP), and other physiological serum parameters were measured using the VetScan VS2 Comprehensive Diagnostic Profile (Abaxis, Inc., Union City, CA).

Histological analysis

Fresh livers were fixed in 10% neutral-buffered formalin, and then subjected to dehydration in different concentrations of alcohol and xylene for paraffin embedding. Four-micrometer serial sections were made through the entire tissue. Histological findings were examined using a light microscope after hematoxylin and eosin staining.

Statistical analysis

Experimental values are presented as mean ± SD. Statistical analysis was performed using GraphPad Prism (San Diego, CA).

The significance of metabolite concentration and mRNA levels was determined using two-tailed Student t-test or the one-way ANOVA with Bonferroni correction for multiple comparisons. P values of less than 0.05 were considered significant.

RESULTS

Phenotypes of *Ppara*-null mice fed with CA diet

Male wild-type and *Ppara*-null mice fed a control diet showed no significant differences in body weight. However, *Ppara*-null mice exhibited significant body weight loss after feeding a CA diet for 12 days, whereas wild-type mice were slightly decreased (**Table 1**). There were no significant differences in food intake and urine volume between the four groups of mice (supplementary Fig. I-A, B). Histological analysis showed severe fatty liver and cholestasis in CA-treated *Ppara*-null mice (**Fig. 1**). In contrast, no fatty liver and cholestasis was induced in wild-type mice fed the CA diet. Further examination indicated that the major lipid composition of hepatic steatosis in CA-treated *Ppara*-null mice was cholesterol and triglyceride (supplementary Fig. II-A, B). In addition, serum chemistry analysis indicated that CA-treated *Ppara*-null mice showed higher ALP, ALT, and serum total bilirubin levels than CA-treated wild-type mice (Table 1). These results indicate that *Ppara*-null mice are susceptible to liver injury induced by dietary CA overload.

Metabolomic analysis of mouse bile, urine, and serum

To gain an understanding for why *Ppara*-null mice were more sensitive to CA challenge than wild-type mice, metabolomic analysis was used to profile the metabolites in the serum, urine, and bile from the four groups. Unsupervised PCA was used to analyze the data sets from the control and CA-fed groups in both wild-type and *Ppara*-null mice. The PCA model shows that bile samples between wild-type and *Ppara*-null mice fed with control or CA diet were distributed in four different quadrants. CA Treatment can significantly increase bile volume in both wild-type and *Ppara*-null mice gallbladder; however, there were no significant differences in bile volume between wild-type and *Ppara*-null mice or between CA-treated wild-type and

TABLE 1. Physiological characteristics and serum chemistry

	Control		CA-Fed	
	Wild-type mice	*Ppara*-null mice	Wild-type mice	*Ppara*-null mice
Body mass (%)	100 ± 10.2	104 ± 1.7	91.1 ± 6.1	67 ± 0.5^a
Liver/body mass (%)	3.2 ± 0.1	3.6 ± 0.2	3.6 ± 0.2	6.1 ± 0.7^a
ALT (U/l)	28.5 ± 4.4	29 ± 8.7	335 ± 148	3660 ± 389^a
ALP (U/l)	104 ± 29.2	65 ± 12.4	67 ± 6.8	396 ± 63.3^a
Glucose (mg/dl)	198 ± 29	150 ± 46.4	157 ± 16.2	85 ± 8.4^a
Total bilirubin (mg/dl)	0.4 ± 0	0.4 ± 0	0.4 ± 0.1	0.7 ± 0.1^b
BUN (mg/dl)	18 ± 3.6	21 ± 3.8	20.5 ± 3.4	30 ± 3.3^a
Potassium (mmol/l)	7.1 ± 0.5	7.7 ± 0.6	7.2 ± 0.5	10.9 ± 0.6^a
Total protein (g/dl)	6 ± 0.7	5.6 ± 0.1	5.6 ± 0.3	4.9 ± 0.2^b

Comparison of diagnostic biomarkers between wild-type and *Ppara*-null mice fed with CA diet (n = 4). The percentage of body weight was calculated by comparing the body weight at day 12 to the starting weight at day 0. The liver/body mass was calculated by comparing the liver weight at day 12 to the body weight at day 12.
$^a P < 0.01.$
$^b P < 0.05.$
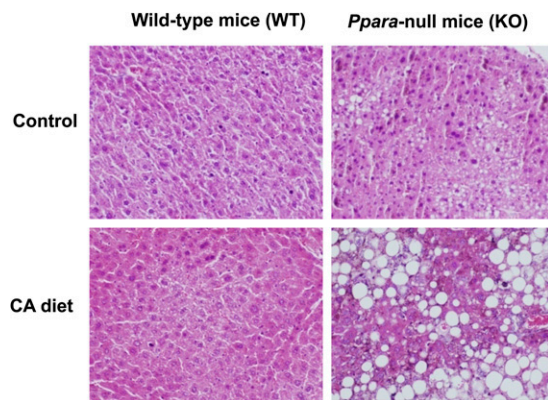
**Fig. 1.** Histological examination of liver. Liver sections were stained by the hematoxylin and eosin method. CA treatment caused severe fatty liver and cholestasis in *Ppara*-null mice, but wild-type mice showed no liver abnormalities following CA treatment.

Ppara-null mice (supplementary Fig. I-C). These data suggested that different bile compositions were present in the four groups of mice (**Fig. 2A**). Significant separation of urine and serum samples were observed in the CA-treated group and control group on day 12 (**Fig. 3A**, B). Compared with the urine sample, a more significant difference was observed between CA-treated *Ppara*-null and wild-type mouse serum in component 1 (X-axis) of the PCA model, suggesting that serum metabolites were more directly affected by CA treatment in *Ppara*-null mice.

After PCA modeling of wild-type and *Ppara*-null mice in the CA- and control-fed groups, a loadings scatter plot revealed ions with the greatest contribution to separation between CA-fed *Ppara*-null mice and other groups. The significant ions increased in *Ppara*-null mice after CA loading were in the first and fourth quadrants, and they decreased in the second and third quadrants (Fig. 3A, B). To identify the ions that contribute to the separation, accurate mass values of each ion were used for chemical formula calculations using element composition and mass-based searches in metabolomics databases (Madison Metabolomics Consortium Database and METLIN). The ions m/z 114.0662^+, 132.0783^+, 139.0500^+, 361.2002^+, 363.2171^+, and 206.0453^+ in urine correspond to creatine, creatinine, nicotinamide 1-oxide, HDOPA, DHOPA, and xanthurenic acid. The ions m/z 407.2795^-, 391.2827^-, 514.2827^-, 514.2820^-, 498.2885^-, 540.3303^-, and 568.3623^- in serum correspond to CA, CDCA, TCA, T-α/β-MCA-MCA, TCDCA, LPC 16:0, and LPC 18:0 (**Table 2**).

Disrupted bile acid homeostasis in CA-treated *Ppara*-null mice

Metabolomic analysis indicated that TCA was the most important ion increased in the serum of CA-fed *Ppara*-null mice. The level of TCA was increased from day 6 of treatment, and the concentration was nearly 16-fold higher at day 12 of treatment in CA-fed *Ppara*-null mice compared with CA-fed wild-type mice (**Fig. 4A**). Along with TCA, CA was markedly elevated in CA-fed *Ppara*-null mice from day 6
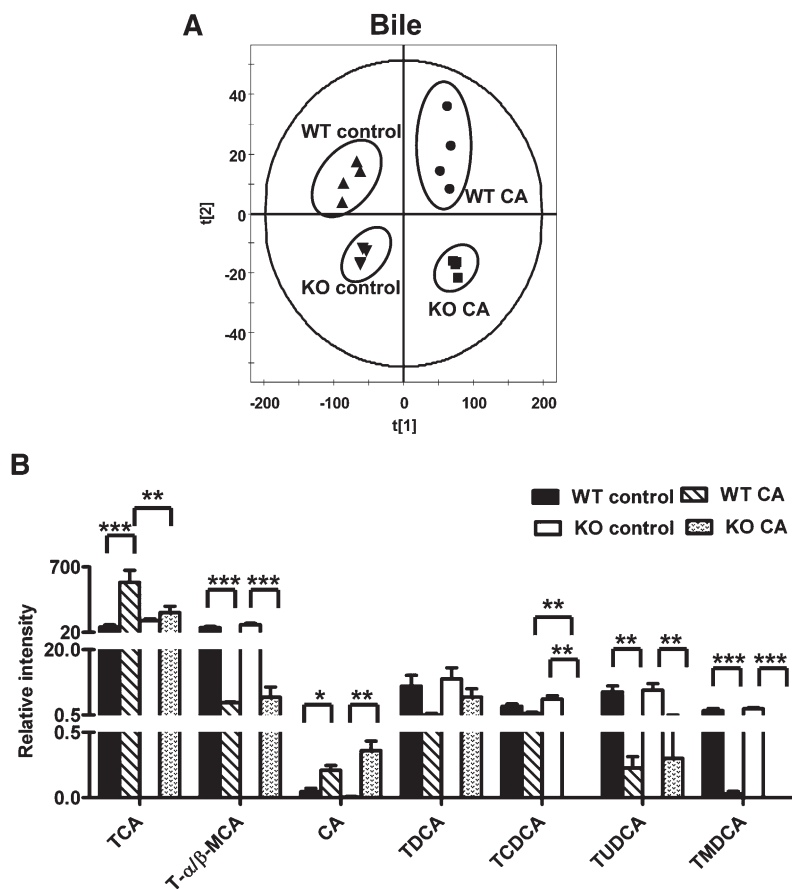
Fig. 2. Metabolomics analysis of bile in control and CA-treated wild-type and *Ppara*-null mice. (A) Scores plot of an PCA model of bile ions from wild-type (WT control, triangle; CA-fed, dot) and *Ppara*-null (KO control, inverted triangle; CA-fed, box) mice fed with control diet or CA diet for 12 days. Each point represents an individual mice bile sample. The t[1] and t[2] correspond to principal components 1 and 2, respectively. Four groups are distributed in four different quadrants of the PCA model. (B) The level of bile acids in bile. *$P < 0.05$; **$P < 0.01$; ***$P < 0.001$.
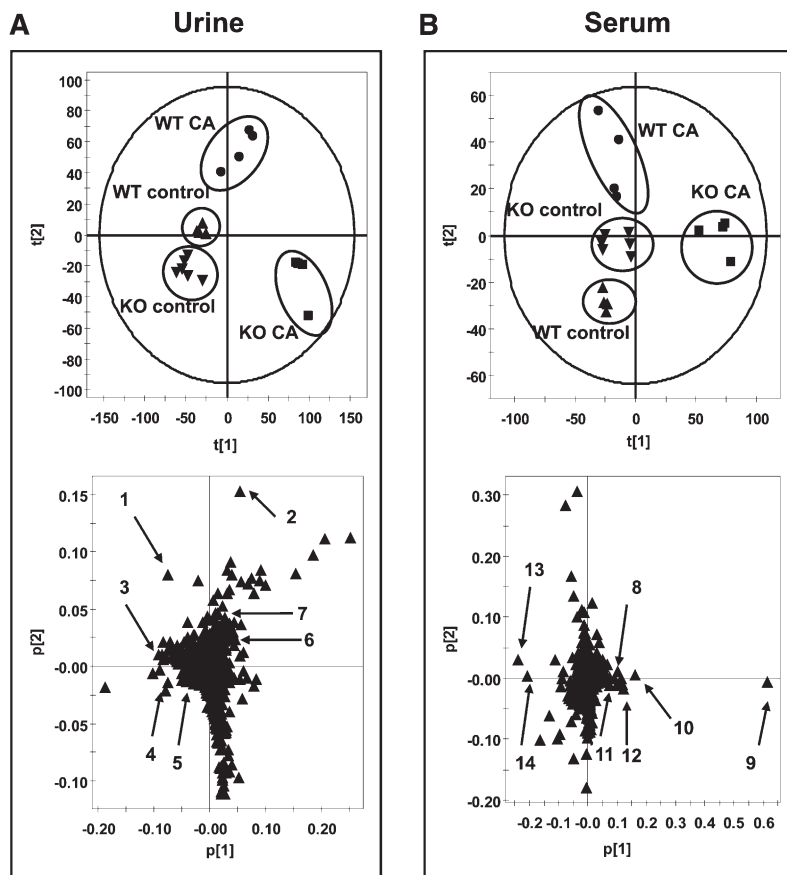
Fig. 3. Identification of urine and serum metabolites significantly altered in *Ppara*-null mice with CA diet treatment using UPLC-ESI-QTOFMS-based metabolomics. (A) Scores plot of a PCA model and PCA loadings scatter plot of urinary ions from wild-type (WT control, triangle; CA-fed, dot) and *Ppara*-null (KO control, inverted triangle; CA-fed, box) mice fed with control diet or 1% CA diet for 12 days. Each point represents an individual mouse urine sample (top) and a urinary ion (bottom). Urine metabolites are labeled in the scatter plot (1–7). (B) Scores plot of an PCA model and PCA loadings scatter plot of serum ions from wild-type (control, closed triangle; CA-fed, closed circle) and *Ppara*-null (control, open triangle; CA-fed, open circle) mice fed with control diet or 1% CA diet for 12 days. Each point represents an individual mouse serum sample (top) and a serum ion (bottom). Serum metabolites are labeled in the scatter plot (8–14). The t[1] and t[2] correspond to principal components 1 and 2, respectively. The p[1] values represent the interclass difference, and p[2] values represent the relative abundance of the ions. Urinary data were obtained in positive mode (ESI$^+$), while serum data were obtained in negative mode (ESI$^-$).

($P < 0.05$) to 12 ($P < 0.01$) (Fig. 4B). On day 12, there was a 25-fold increase in CA-treated *Ppara*-null mice compared with CA-treated wild-type mice. In addition, the levels of serum CDCA, T-α/β-MCA, and TCDCA were increased at day 12 of treatment in *Ppara*-null mice fed with CA diet (data no shown). Further gene expression analysis indicated that the major enzymes involved in the bile acid biosynthesis, including Cyp7a1, Cyp7b1, Cyp8b1, Cyp27a1, and hydroxy-delta-5-steroid dehydrogenase 3b7 (Hsd3b7) were decreased in the CA-fed *Ppara*-null mice at day 12 of treatment compared with CA-treated wild-type mice and

untreated *Ppara*-null mice (Fig. 4C). Two enzymes involved in the bile acid conjugation, bile acid-CoA synthetase (Bacs, also called Slc27a5) and bile acid-CoA amino acid *N*-acetyltransferase (Baat), were significantly diminished in the liver of CA-fed *Ppara*-null mice. The bile acid transporters sodium-taurocholate cotransporting polypeptide (Ntcp), anion transporting polypeptide 1 (Oatp1), and anion transporting polypeptide 4 (Oatp4), which absorb bile acids from blood into liver, were decreased in *Ppara*-null mice, whereas the transporter Abcc4, which carries bile acids from liver to blood, was dramatically increased

TABLE 2. Summary of ions altered in CA-treated *Ppara*-null mice compared with CA-treated wild-type mice

| No	RT (min)	Mass (*m/z*)	Empirical Formula	Mass Error (ppm)	Identity	Up/Down	Fold Change
Urine							
1	0.32	132.0783	C4H9N3O2 [H+]	7.6	Creatine	↑	8.4
2	0.31	114.0662	C4H7N3O [H+]	−4.4	Creatinine	↓	2.6
3	1.80	206.0453	C10H7NO4 [H+]	0	Xanthurenic acid	↓	3.2
4	0.33	139.0500	C6H6N2O2 [H+]	−5.7	Nicotinamide 1-oxide	↓	8.3
5	2.61	194.0812	C10H11NO3 [H+]	−2.5	Phenylacetylglycine	↓	3.9
6	5.33	361.2002	C21H28O5 [H+]	−3.6	HDOPA	↑	20
7	5.22	363.2171	C21H30O5 [H+]	0	DHOPA	↑	3.6
Serum							
8	3.53	407.2795	C24H40O5 [H−]	−0.5	CA	↑	25
9	2.92	514.2827	C26H45NO7S [H−]	−2.1	TCA	↑	16
10	2.56	514.2820	C26H45NO7S [H−]	−3.5	T-α/β-MCA	↑	12
11	4.13	391.2827	C24H40O4 [H−]	−5.3	CDCA	↑	7
12	3.40	498.2885	C26H45NO6S [H−]	−0.8	TCDCA	↑	10
13	5.38	568.3623	C27H56NO9P [H−]	1.6	LPC 18:0	↓	1.6
14	4.76	540.3303	C25H52NO9P [H−]	0.4	LPC 16:0	↓	1.6

↑, upregulation; ↓, downregulation.
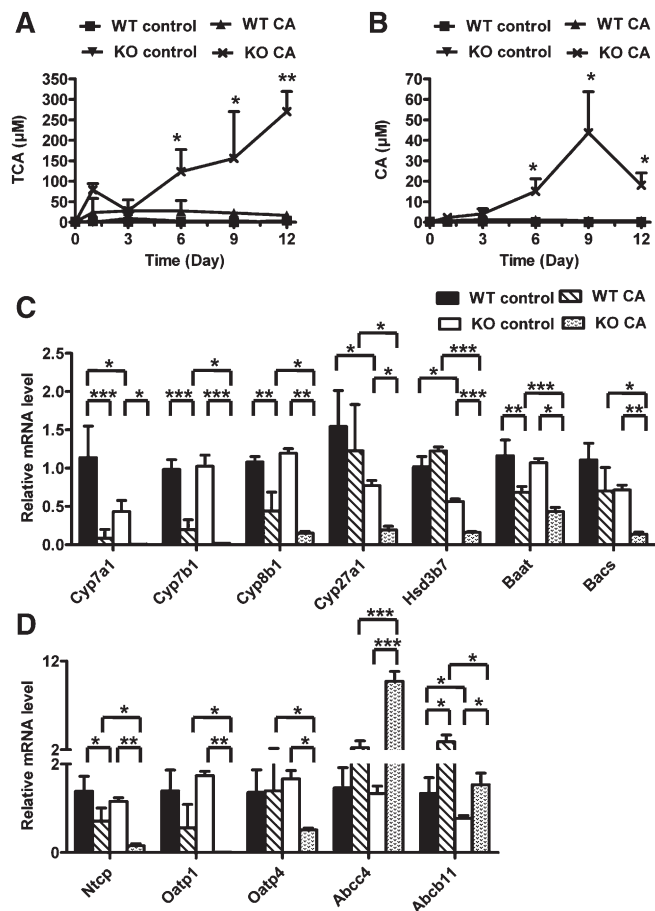
Fig. 4. Effect of CA diet on bile acid metabolism in *Ppara*-null mice. (A, B) Serum levels of CA (A) and TCA (B) between wild-type (WT) and *Ppara*-null (KO) mice fed with control diet and CA diet from day 0 to 12. (C) Hepatic mRNA levels of genes associated with bile acid biosynthesis and transport in mice with day 12 of treatment. *$P < 0.05$; **$P < 0.01$; ***$P < 0.001$.

(Fig. 4D). In addition, the mRNA encoding bile acid transporter ATP-binding cassette subfamily B member 11 (Abcb11, also called Bsep) located in liver canaliculus that transports bile acids from liver to bile duct, was increased by CA treatment in wild-type and *Ppara*-null mice. However, lower levels of Abcb11 were observed in CA-treated *Ppara*-null mice compared with CA-treated wild-type mice. Metabolomic analysis of bile indicated that CA treatment significantly changes the bile acid composition of bile in both wild-type and *Ppara*-null mice, notably T-α/β-MCA, TUDCA, and TMDCA (Fig. 2B). Since CA treatment significantly altered the bile volume in both wild-type and *Ppara*-null mice, the relative concentrations of bile acids in bile were determined (Fig. 2B). However, compared with CA-treated wild-type mice, TCA and TCDCA were lower in CA-treated *Ppara*-null mice. These results suggested that the bile acid homeostasis was markedly disrupted in CA-treated *Ppara*-null mice compared with CA-treated wild-type mice and control mice.

Alteration of phospholipid homeostasis in CA-treated *Ppara*-null mice

Along with the accumulation of bile acids, metabolomic analysis showed the decreased levels of two phospholipids,

LPC 16:0 and LPC 18:0 in the serum of CA-treated *Ppara*-null mice. Triplequadrupole quantitation further confirmed that the level of LPC 16:0 was decreased in CA-treated *Ppara*-null mice from day 3 ($P < 0.05$) to 12 ($P < 0.01$) (**Fig. 5A**). Compared with LPC 16:0, the level of LPC 18:0 was significantly reduced in CA-treated *Ppara*-null mice on day 12 ($P < 0.05$) (Fig. 5B). On day 12, there was a 1.6-fold depletion of both phospholipids in CA-treated *Ppara*-null mice compared with CA-treated wild-type mice. Phospholipids have been reported to be biomarkers for LCA induced cholestasis (19). Liver gene expression indicated that the mRNAs encoding enzymes involved in the LPC biosynthesis [lecithin-cholesterol acyltransferase (Lcat), phosphate cytidylyltransferase 1 (Pcyt1α), choline phosphotransferase 1 (Chpt1), and choline kinase β (Chkβ)] were significantly decreased in CA-treated *Ppara*-null mice compared with CA-treated wild-type mice and untreated *Ppara*-null mice (Fig. 5C). Similarly, the expression of mRNAs encoding proteins associated with LPC metabolism [lysophosphatidylcholine acyltransferase 3 (Lpcat3), lysophospholipase A1 (Lyp1a1), and ectonucleotide pyrophosphatase/ phosphodiesterase 2 (Enpp2)] were reduced in CA-treated *Ppara*-null mice (Fig. 5C). In addition, the mRNA encoding the phospholipid transporter ATP-binding cassette subfamily B member 4 (Abcb4) located in the liver canaliculus, was diminished in CA-treated *Ppara*-null mice compared with CA-treated wild-type mice. These data indicate that phospholipids homeostasis was also disrupted in CA-treated *Ppara*-null mice.
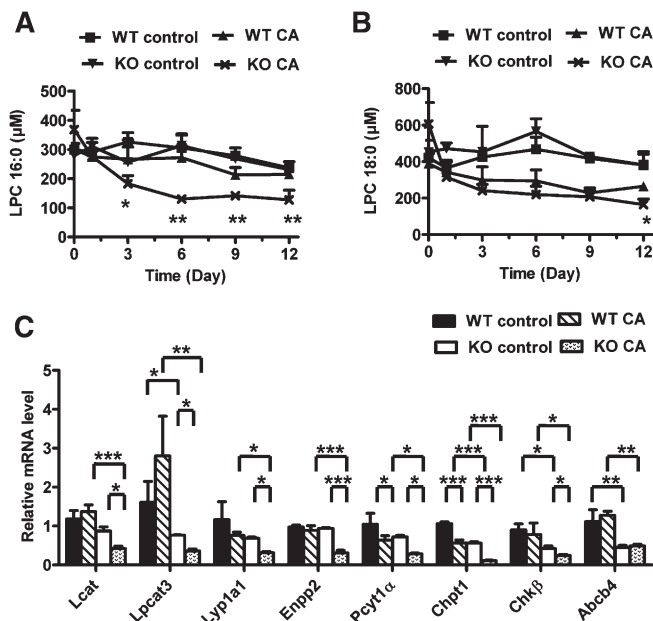
Fig. 5. Effect of CA diet on phospholipid metabolism in *Ppara*-null mice. (A, B) Serum levels of LPC 16:0 (A) and 18:0 (B) between wild-type (WT) and *Ppara*-null (KO) mice fed control diet and CA diet from day 0 to 12. (C) Hepatic mRNA levels of genes associated with LPC biosynthesis, metabolism, and transport in mice with day 12 of treatment. *$P < 0.05$; **$P < 0.01$; ***$P < 0.001$.
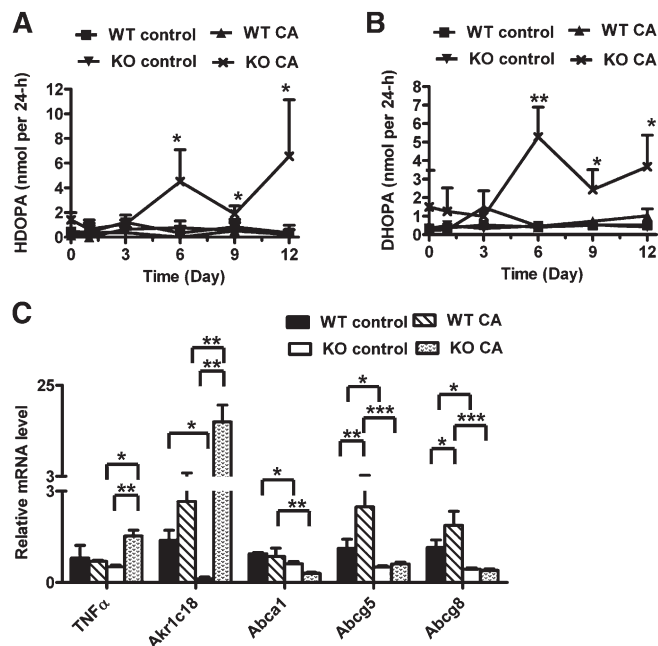
Change in cholesterol and corticosterone metabolism in CA-treated *Ppara*-null mice

The generation of bile acids from cholesterol is a metabolic pathway for cholesterol degradation in vivo. To determine whether other metabolic pathways involving cholesterol were also affected, the metabolites associated with cholesterol and steroid hormone metabolism were examined in serum and urine. Although there was no significant change in serum corticosterone and progesterone levels (supplementary Fig. III), two corticosterone derivatives, HDOPA and DHOPA, showed a significant increase in urine of CA-treated *Ppara*-null mice (**Fig. 6A**, B). Both metabolites were significantly increased from day 6 to 12. On day 12, HDOPA and DHOPA were increased by 20- and 3.6-fold, respectively, in CA-treated *Ppara*-null mice compared with CA-treated wild-type mice. In addition, hepatic expression levels of the PPARα target gene aldo-keto reductase family 1c18 (Akr1c18) was significantly diminished in the control diet-treated *Ppara*-null mice compared with wild-type mice (20). The mRNA encoding Akr1c18 involved in the generation of HDOPA and DHOPA was greatly increased (6-fold) in CA-treated *Ppara*-null mice (Fig. 6C), whereas genes associated with corticosterone metabolism, such as aldo-keto reductase family 1c14 (Akr1c14), steroid 5 α-reductase 1 (Srd5a1), hydroxysteroid (17-β) dehydrogenase 3 (Hsd17b3), and aldehyde dehydrogenase family 3, subfamily A2 (Aldh3a2), were decreased (supplementary Fig. IV). These data suggested that enhanced Akr1c18 expression was responsible for the increase of HDOPA and DHOPA in the CA-treated *Ppara*-

null mice urine. In addition, three cholesterol transporters, ATP-binding cassette subfamily A member 1 (Abca1), ATP-binding cassette subfamily G member 5 (Abcg5), and ATP-binding cassette subfamily G member 8 (Abcg8), were significantly decreased in CA-treated *Ppara*-null mice compared with CA-treated wild-type mice. Although the mRNA levels of Abcg5 and Abcg8 are elevated by CA treatment in wild-type mice, there was no significant difference between CA-treated and untreated *Ppara*-null mice.

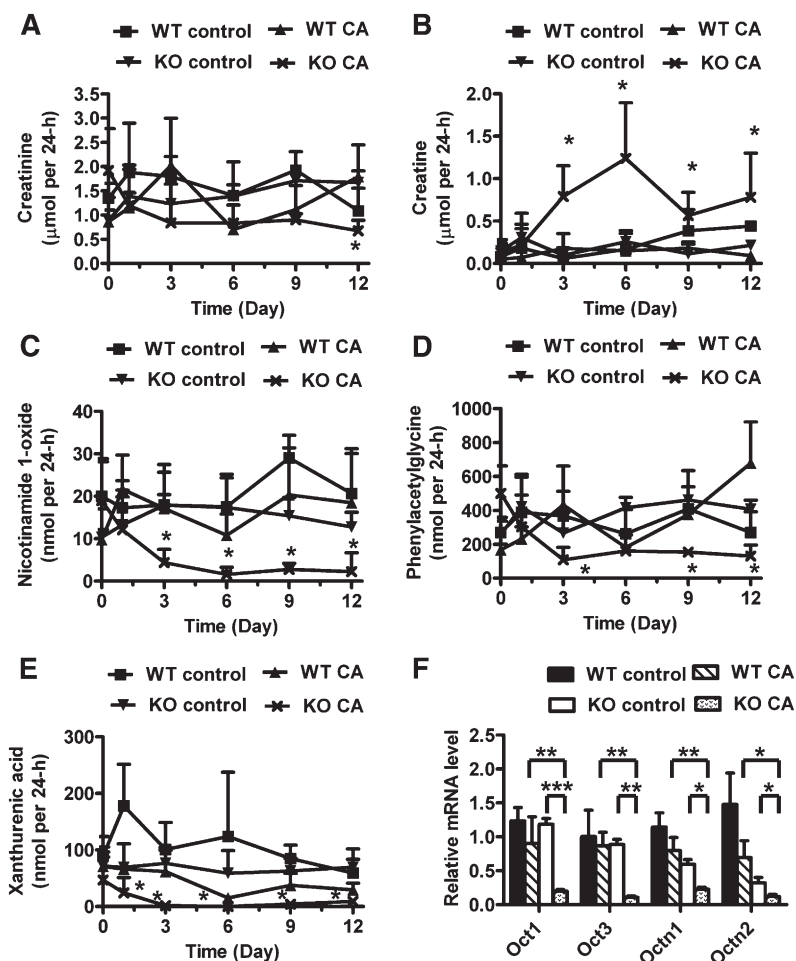## Disorder of cation and anion transport in CA-treated *Ppara*-null mice

Along with the increase in the HDOPA and DHOPA excretion, metabolomic analysis revealed altered levels of endogenous cationic and anionic metabolites, such as nicotinamide 1-oxide and xanthurenic acid, in urine of CA-treated *Ppara*-null mice. As shown in **Fig. 7A**, the excretion of creatinine was significantly decreased in CA-treated *Ppara*-null mice. Therefore, the level of urinary metabolites was presented as total mass in 24 h. The excretion of creatine, one endogenous cation, was significantly increased in CA-treated *Ppara*-null mice from day 3 ($P < 0.05$) to 12 ($P < 0.05$) (Fig. 7B), whereas creatinine excretion was decreased on day 12 ($P < 0.05$) (Fig. 7A). The excretion of another cation nicotinamide 1-oxide also was significantly reduced from day 3 ($P < 0.05$) to 12 ($P < 0.05$) (Fig. 7C). Similarly, the urinary excretion of two endogenous anion metabolites, phenylacetylglycine (3.9-fold) and xanthurenic acid (3.2-fold), was decreased in CA-treated *Ppara*-null mice on day 12 (Fig. 7D, E). qPCR analysis indicated that the expression of several organic cation transporters (Octs) and organic anion transporters (Oats) was dramatically diminished in the liver and kidney of CA-treated *Ppara*-null mice compared with untreated *Ppara*-null mice and CA-treated wild-type mice, including organic cation transporter 1 (Oct1/Slc22A1), organic cation transporter 2 (Oct2/Slc22A2), organic cation transporter 3 (Oct3/Slc22A3), organic cation/carnitine transporter 1 (Octn1/Slc22A4), organic cation/carnitine transporter 2 (Octn2/Slc22A5), Oatp1, and Oatp4 (Figs. 3D and 7F and supplementary Fig. V). These results demonstrated that CA challenge also leads to a disruption of endogenous cation and anion transport in *Ppara*-null mice.

DISCUSSION

To clarify the functional role of PPARα in bile acid homeostasis, the present study investigated the change in endogenous metabolites and associated genes in *Ppara*-null mice during exposure to a CA diet. Metabolomics indicated disruption of bile acid homeostasis, phospholipid homeostasis, cholesterol metabolism, and endogenous cations and anions transport in CA-treated *Ppara*-null mice. Further gene expression analysis revealed that the bile acid disorder in CA-treated *Ppara*-null mice might be due to a deficiency in expression of the Abc transporters (Abcb11, Abcb4, Abca1, Abcg5, and Abcg8) in the liver caniculus. Additionally, the levels of bile acid synthesis enzymes (Cyp7a1, Cyp27a1, and Hsd3b7) were lower in untreated

Fig. 6. Effect of CA diet on cholesterol and corticosterone metabolism in *Ppara*-null mice. (A, B) Urinary excretion of HDOPA (A) and DHOPA (B) between wild-type (WT) and *Ppara*-null (KO) mice fed with control diet and CA diet from day 0 to 12. (C) Hepatic mRNA level of genes associated with corticosterone metabolism and cholesterol transport in mice with day 12 of treatment. *$P < 0.05$; **$P < 0.01$; ***$P < 0.001$.

Fig. 7. Effect of CA diet on endogenous cations and anions transport in *Ppara*-null mice. (A–E) Urinary excretion of creatinine (A), creatine (B), nicotinamide 1-oxide (C), phenylacetylglycine (D), and xanthurenic acid (E) between wild-type (WT) and *Ppara*-null (KO) mice fed with control diet and CA diet in 24 h from day 0 to 12. (F) Hepatic mRNA levels of organic cation transporters (Octs) in mice with day 12 of treatment. $*P < 0.05$; $**P < 0.01$; $***P < 0.001$.

Ppara-null mice than in untreated wild-type mice. These results demonstrated that PPARα regulates bile acid homeostasis not only via its effect on bile acid biosynthesis and transport but also via its effect on biliary secretion.

When *Ppara*-null mice were treated with a CA diet, one significant observation was liver injury. The change in phenotype of the CA-treated *Ppara*-null mice included body weight loss, enhanced serum ALP and ALT levels, and cholestasis. These phenotypes are similar with those previously reported for the farnesoid X receptor (*Fxr*)-null mice after feeding CA (21). In addition, higher total bilirubin and lower glucose levels were also observed in CA-fed *Ppara*-null mice. Further metabolomic analysis revealed an alteration of three important metabolic pathways, bile acid metabolism, phospholipid metabolism, and cholesterol metabolism, in CA-treated *Ppara*-null mice. First, a high level of bile acids, including CA, CDCA, TCA, T-α/β-CA, and TCDCA, were noted in CA-treated *Ppara*-null mouse serum, and the genes involved in bile acid synthesis and transport were diminished in the liver, thus suggesting significant liver injury after feeding *Ppara*-null mice CA. Numerous studies have demonstrated that increased levels of serum bile acids were induced in cholestasis models (16, 22, 23). Second, two phospholipids, LPC 16:0 and LPC 18:0, were decreased in CA-treated *Ppara*-null mice serum. LPCs, which are derived from phosphatidylcholine by hydrolysis, are the major phospholipid species in serum. Phospholipids

are important components in bile that are sensitive to liver bile acid levels. In the clinic, abnormal levels of serum LPCs are typically associated with liver injury (24, 25). Similarly, it was reported that a series of LPCs were significantly decreased in cholestasis induced by LCA treatment and nonalcoholic steatohepatitis induced by methionine- and choline-deficient diet treatment (19, 26). Third, the excretion of HDOPA and DHOPA was increased in the CA-treated *Ppara*-null mice urine. HDOPA and DHOPA were generated from corticosterone under the effect of cytochrome P450s (Cyps), which was confirmed by in vitro and in vivo experiments (9, 20). Recently, HDOPA and DHOPA were reported as biomarkers for PPARα activation (9). However, the expression of PPARα target genes suppressed in *Ppara*-null mice suggested that the increase in both metabolites in this study was not likely due to the activation of PPARα. It was reported that in cholestatic animals and humans, the hypothalamic-pituitary-adrenal axis can be activated by endotoxin and cytokines, such as tumor necrosis factor α (TNFα), resulting in the elevation of glucocorticoids (27). Two studies indicated that the excretion of HDOPA and DHOPA was increased in the hepatotoxicity model of hepatocyte nuclear factor 1α (*Hnf1α*)-null mice (28) and CA-treated *Fxr*-null mice (21). Here, the expression of TNFα was activated in CA-treated *Ppara*-null mice, suggesting that accelerated corticosterone metabolism in CA-treated *Ppara*-null mice also results from liver

cholestasis. The change in the bile acids, phospholipids, and cholesterol homeostasis provides compelling evidence that hepatotoxicity was induced in *Ppara*-null mice in response to CA challenge.

Another observation in this study is the disrupted transport of endogenous cations and anions in the liver and kidney. The possibility exists that altered levels of creatine, creatinine, and nicotinamide 1-oxide observed in the CA-treated *Ppara*-null mice is due to inhibition of Octs function in vivo. In the liver and kidney, the Octs family mediates the reabsorption and excretion of various cationic compounds, including endogenous cations (choline and carnitine), cationic toxins (1-methyl-4-phenylpyridium), and cationic drugs (quinidine and procainamide) (29). Several studies have shown that Oct2 plays an important role in renal secretion of creatinine in humans and mice (30, 31). Additionally, methylnicotinamide, used as a model substrate for studying organic cation transport, can be regulated by Oct1 and Oct2 (32, 33). In vivo, nicotinamide 1-oxide and methylnicotinamide are derived from nicotinamide. These studies suggest that inhibition of Octs might directly affect the transport of creatinine, creatine, and nicotinamide 1-oxide in vivo. Additionally, two organic anionic metabolites, phenylacetylglycine and xanthurenic acid, were significantly decreased in CA-treated *Ppara*-null mice. A recent study using untargeted metabolomics revealed that both metabolites were identified as biomarkers associated with the deficiency of Oat1 (34). Another earlier study conducted by gas chromatography-mass spectrometry (GC-MS), also indicated that the excretion of endogenous organic anions was decreased in Oat1 knockout mouse urine (35). Here, CA treatment decreased Oatp1 and Oatp4 in CA-fed *Ppara*-null mouse liver and kidney. Oatp1 mRNA is found in various tissues (36) including the liver, kidney, and brain, whereas Oatp4 is exclusively in the liver (37). Along with the transport of bile acids, both transporters play a major role in the uptake and secretion of other organic anions in the kidney and liver, such as bromosulfophthalein and estrone sulfate (38, 39). Thus, it is likely that the diminished expression of Oatp1 and Oatp4 in the liver and kidney is responsible for the decrease of phenylacetylglycine and xanthurenic acid in urine.

Previous studies have demonstrated that the activation/repression of PPARα can affect bile acid biosynthesis. However, different activators, such as Wy-14,643 and fibrates, show completely different effects on the rate-limiting enzyme in bile acid synthesis enzyme Cyp7a1 (3-5). Compared with fenofibrate and other fibrates, Wy-14,643 is a more potent ligand of PPARα. One possible reason for different effects is that the level of Cyp7a1 might be regulated by other nuclear receptors, such as liver X receptor (LXR) (40) and hepatocyte nuclear factor 4α (HNF4α), during the activation of PPARα (41, 42). In this study, in comparison with control diet-treated wild-type mice, the enzymes involved in biosynthesis of bile acids from cholesterol were reduced in control diet-treated *Ppara*-null mice, including Cyp7a1, Cyp27a1, and Hsd3b7. One early study reported that the mRNA level of Cyp7a1 also could be reduced in *Ppara*-null mice compared with wild-type mice (3).

Although earlier studies showed that ciprofibrate (43) and perfluorinated fatty acids (7) cause a decrease in hepatic transporters Ntcp and Oatp1, the level of Ntcp and Oatps were unchanged in control diet-treated *Ppara*-null mice compared with wild-type mice. In the liver, the expression of Abcb11 was decreased in control diet-treated *Ppara*-null mice, consistent with the observations that *Ppara*-null mice show lower hepatic Abcb11 level than wild-type mice (5). Thus, the deficiency of PPARα can directly affect the bile acid transporter Abcb11 in the liver. More importantly, the mRNA levels of the phospholipid transporter Abcb4 and cholesterol transporters Abca1, Abcg5, and Abcg8 also were diminished in the liver following knockout of PPARα. Various studies have indicated that treatment with Wy-14,643 and other PPARα activators can stimulate the expression of Abcb4, Abca1, Abcg5, and Abcg8 (43–45). Actually, it was reported that PPARα can regulate hepatic lipid homeostasis via its target effect on these Abc transporters (46, 47). During CA challenge, the reduced mRNA expression of these Abc transporters greatly affected the transport of bile acids in *Ppara*-null mice, finally causing severe liver cholestasis. Taken together, the deficiency of PPARα can cause decreased bile acid biosynthesis, transport, and secretion.

Although the expression of several genes involved in the bile acid metabolism was reduced in *Ppara*-null mice, metabolomics did not reveal abnormal bile acid levels in untreated urine and serum in these mice. To better evaluate the role of PPARα in the regulation of bile acid homeostasis, CA challenge was conducted in *Ppara*-null mice. The results showed severe hepatotoxicity in *Ppara*-null mice during CA challenge that was not observed in wild-type mice. Numerous studies have reported that CA challenge can lead to severe liver injury in transgenic mice in which specific genes involved in bile acid metabolism had been knocked out, such as *Fxr*-null mice (48), *Abcb11*-null mice (49), and *Shp*-null mice (50). The current studies demonstrated a key role of PPARα in the regulation of bile acid homeostasis. The hepatotoxicity in CA-treated *Ppara*-null mice might be due to the decrease in expression of the Abc transporters in the liver canaliculus. The reduced biliary secretion causes the accumulation of bile acids in *Ppara*-null mice liver during CA exposure. Indeed, a metabolic disorder was observed in CA-treated *Ppara*-null by metabolomics, including altered bile acid metabolism, phospholipid metabolism, cholesterol metabolism, and transport of endogenous cations and anions. The data presented herein demonstrate the power of mass spectrometry-based metabolomic analysis in combination with traditional serum chemistry analysis and histological examination using a transgenic mouse model to profile metabolic pathways and uncover the physiological function of nuclear receptor.

REFERENCES

1. Inagaki, T., P. Dutchak, G. Zhao, X. Ding, L. Gautron, V. Parameswara, Y. Li, R. Goetz, M. Mohammadi, V. Esser, et al. 2007. Endocrine regulation of the fasting response by PPARalpha-mediated induction of fibroblast growth factor 21. *Cell Metab.* **5:** 415–425.

2. Mandard, S., M. Muller, and S. Kersten. 2004. Peroxisome proliferator-activated receptor alpha target genes. *Cell. Mol. Life Sci.* **61:** 393–416.

3. Hunt, M. C., Y. Z. Yang, G. Eggertsen, C. M. Carneheim, M. Gafvels, C. Einarsson, and S. E. Alexson. 2000. The peroxisome proliferator-activated receptor alpha (PPARalpha) regulates bile acid biosynthesis. *J. Biol. Chem.* **275:** 28947–28953.

4. Cheema, S. K., and L. B. Agellon. 2000. The murine and human cholesterol 7alpha-hydroxylase gene promoters are differentially responsive to regulation by fatty acids mediated via peroxisome proliferator-activated receptor alpha. *J. Biol. Chem.* **275:** 12530–12536.

5. Hays, T., I. Rusyn, A. M. Burns, M. J. Kennett, J. M. Ward, F. J. Gonzalez, and J. M. Peters. 2005. Role of peroxisome proliferator-activated receptor-alpha (PPARalpha) in bezafibrate-induced hepatocarcinogenesis and cholestasis. *Carcinogenesis.* **26:** 219–227.

6. Post, S. M., H. Duez, P. P. Gervois, B. Staels, F. Kuipers, and H. M. Princen. 2001. Fibrates suppress bile acid synthesis via peroxisome proliferator-activated receptor-alpha-mediated downregulation of cholesterol 7alpha-hydroxylase and sterol 27-hydroxylase expression. *Arterioscler. Thromb. Vasc. Biol.* **21:** 1840–1845.

7. Cheng, X., and C. D. Klaassen. 2008. Critical role of PPAR-alpha in perfluorooctanoic acid- and perfluorodecanoic acid-induced downregulation of Oatp uptake transporters in mouse livers. *Toxicol. Sci.* **106:** 37–45.

8. Jung, D., M. Fried, and G. A. Kullak-Ublick. 2002. Human apical sodium-dependent bile salt transporter gene (SLC10A2) is regulated by the peroxisome proliferator-activated receptor alpha. *J. Biol. Chem.* **277:** 30559–30566.

9. Zhen, Y., K. W. Krausz, C. Chen, J. R. Idle, and F. J. Gonzalez. 2007. Metabolomic and genetic analysis of biomarkers for peroxisome proliferator-activated receptor alpha expression and activation. *Mol. Endocrinol.* **21:** 2136–2151.

10. Patterson, A. D., J. A. Bonzo, F. Li, K. W. Krausz, G. S. Eichler, S. Aslam, X. Tigno, J. N. Weinstein, B. C. Hansen, J. R. Idle, et al. 2011. Metabolomics reveals attenuation of the SLC6A20 kidney transporter in nonhuman primate and mouse models of type 2 diabetes mellitus. *J. Biol. Chem.* **286:** 19511–19522.

11. Li, F., A. D. Patterson, C. C. Hofer, K. W. Krausz, F. J. Gonzalez, and J. R. Idle. 2011. A comprehensive understanding of thioTEPA metabolism in the mouse using UPLC-ESI-QTOFMS-based metabolomics. *Biochem. Pharmacol.* **81:** 1043–1053.

12. Li, F., A. D. Patterson, C. C. Hofer, K. W. Krausz, F. J. Gonzalez, and J. R. Idle. 2010. Comparative metabolism of cyclophosphamide and ifosfamide in the mouse using UPLC-ESI-QTOFMS-based metabolomics. *Biochem. Pharmacol.* **80:** 1063–1074.

13. Patterson, A. D., O. Slanar, K. W. Krausz, F. Li, C. C. Hofer, F. Perlik, F. J. Gonzalez, and J. R. Idle. 2009. Human urinary metabolomic profile of PPARalpha induced fatty acid beta-oxidation. *J. Proteome Res.* **8:** 4293–4300.

14. Chen, C., K. W. Krausz, Y. M. Shah, J. R. Idle, and F. J. Gonzalez. 2009. Serum metabolomics reveals irreversible inhibition of fatty acid beta-oxidation through the suppression of PPARalpha activation as a contributing mechanism of acetaminophen-induced hepatotoxicity. *Chem. Res. Toxicol.* **22:** 699–707.

15. Sinal, C. J., M. Tohkin, M. Miyata, J. M. Ward, G. Lambert, and F. J. Gonzalez. 2000. Targeted disruption of the nuclear receptor FXR/BAR impairs bile acid and lipid homeostasis. *Cell.* **102:** 731–744.

16. Teng, S., and M. Piquette-Miller. 2007. Hepatoprotective role of PXR activation and MRP3 in cholic acid-induced cholestasis. *Br. J. Pharmacol.* **151:** 367–376.

17. Song, P., Y. Zhang, and C. D. Klaassen. 2011. Dose-response of five bile acids on serum and liver bile Acid concentrations and hepatotoxicty in mice. *Toxicol. Sci.* **123:** 359–367.

18. Kind, T., and O. Fiehn. 2007. Seven Golden Rules for heuristic filtering of molecular formulas obtained by accurate mass spectrometry. *BMC Bioinformatics.* **8:** 105.

19. Matsubara, T., N. Tanaka, A. D. Patterson, J. Y. Cho, K. W. Krausz, and F. J. Gonzalez. 2011. Lithocholic acid disrupts phospholipid and sphingolipid homeostasis leading to cholestasis in mice. *Hepatology.* **53:** 1282–1293.

20. Wang, T., Y. M. Shah, T. Matsubara, Y. Zhen, T. Tanabe, T. Nagano, S. Fotso, K. W. Krausz, T. M. Zabriskie, J. R. Idle, et al. 2010. Control of steroid 21-oic acid synthesis by peroxisome proliferator-activated receptor alpha and role of the hypothalamic-pituitary-adrenal axis. *J. Biol. Chem.* **285:** 7670–7685.

21. Cho, J. Y., T. Matsubara, D. W. Kang, S. H. Ahn, K. W. Krausz, J. R. Idle, H. Luecke, and F. J. Gonzalez. 2010. Urinary metabolomics in Fxr-null mice reveals activated adaptive metabolic pathways upon bile acid challenge. *J. Lipid Res.* **51:** 1063–1074.

22. Fiorucci, S., C. Clerici, E. Antonelli, S. Orlandi, B. Goodwin, B. M. Sadeghpour, G. Sabatino, G. Russo, D. Castellani, T. M. Willson, et al. 2005. Protective effects of 6-ethyl chenodeoxycholic acid, a farnesoid X receptor ligand, in estrogen-induced cholestasis. *J. Pharmacol. Exp. Ther.* **313:** 604–612.

23. Jansen, P. L., S. S. Strautnieks, E. Jacquemin, M. Hadchouel, E. M. Sokal, G. J. Hooiveld, J. H. Koning, A. De Jager-Krikken, F. Kuipers, F. Stellaard, et al. 1999. Hepatocanalicular bile salt export pump deficiency in patients with progressive familial intrahepatic cholestasis. *Gastroenterology.* **117:** 1370–1379.

24. Yang, J., X. Zhao, X. Liu, C. Wang, P. Gao, J. Wang, L. Li, J. Gu, S. Yang, and G. Xu. 2006. High performance liquid chromatography-mass spectrometry for metabonomics: potential biomarkers for acute deterioration of liver function in chronic hepatitis B. *J. Proteome Res.* **5:** 554–561.

25. Yin, P., D. Wan, C. Zhao, J. Chen, X. Zhao, W. Wang, X. Lu, S. Yang, J. Gu, and G. Xu. 2009. A metabonomic study of hepatitis B-induced liver cirrhosis and hepatocellular carcinoma by using RP-LC and HILIC coupled with mass spectrometry. *Mol. Biosyst.* **5:** 868–876.

26. Tanaka, N., T. Matsubara, K. W. Krausz, A. D. Patterson, and F. J. Gonzalez. Disruption of phospholipid and bile acid homeostasis in mice with nonalcoholic steatohepatitis. *Hepatology.* Epub ahead of print. January 30, 2012; doi:10.1002/hep.25630.

27. Swain, M. G., and M. Maric. 1996. Tumor necrosis factor-alpha stimulates adrenal glucocorticoid secretion in cholestatic rats. *Am. J. Physiol.* **270:** G987–G991.

28. Bonzo, J. A., A. D. Patterson, K. W. Krausz, and F. J. Gonzalez. 2010. Metabolomics identifies novel Hnf1alpha-dependent physiological pathways in vivo. *Mol. Endocrinol.* **24:** 2343–2355.

29. Kato, Y., Y. Kubo, D. Iwata, S. Kato, T. Sudo, T. Sugiura, T. Kagaya, T. Wakayama, A. Hirayama, M. Sugimoto, et al. 2010. Gene knockout and metabolome analysis of carnitine/organic cation transporter OCTN1. *Pharm. Res.* **27:** 832–840.

30. Urakami, Y., N. Kimura, M. Okuda, and K. Inui. 2004. Creatinine transport by basolateral organic cation transporter hOCT2 in the human kidney. *Pharm. Res.* **21:** 976–981.

31. Ciarimboli, G., C. S. Lancaster, E. Schlatter, R. M. Franke, J. A. Sprowl, H. Pavenstadt, V. Massmann, D. Guckel, R. H. Mathijssen, W. Yang, et al. 2012. Proximal tubular secretion of creatinine by organic cation transporter OCT2 in cancer patients. *Clin. Cancer Res.* **18:** 1101–1108.

32. Green, R. M., K. Lo, C. Sterritt, and D. R. Beier. 1999. Cloning and functional expression of a mouse liver organic cation transporter. *Hepatology.* **29:** 1556–1562.

33. Urakami, Y., M. Okuda, S. Masuda, H. Saito, and K. I. Inui. 1998. Functional characteristics and membrane localization of rat multispecific organic cation transporters, OCT1 and OCT2, mediating tubular secretion of cationic drugs. *J. Pharmacol. Exp. Ther.* **287:** 800–805.

34. Wikoff, W. R., M. A. Nagle, V. L. Kouznetsova, I. F. Tsigelny, and S. K. Nigam. 2011. Untargeted metabolomics identifies enterobiome metabolites and putative uremic toxins as substrates of organic anion transporter 1 (Oat1). *J. Proteome Res.* **10:** 2842–2851.

35. Eraly, S. A., V. Vallon, D. A. Vaughn, J. A. Gangoiti, K. Richter, M. Nagle, J. C. Monte, T. Rieg, D. M. Truong, J. M. Long, et al. 2006. Decreased renal organic anion secretion and plasma accumulation of endogenous organic anions in OAT1 knock-out mice. *J. Biol. Chem.* **281:** 5072–5083.

36. Bergwerk, A. J., X. Shi, A. C. Ford, N. Kanai, E. Jacquemin, R. D. Burk, S. Bai, P. M. Novikoff, B. Stieger, P. J. Meier, et al. 1996. Immunologic distribution of an organic anion transport protein in rat liver and kidney. *Am. J. Physiol.* **271:** G231–G238.

37. Cattori, V., J. E. van Montfoort, B. Stieger, L. Landmann, D. K. Meijer, K. H. Winterhalter, P. J. Meier, and B. Hagenbuch. 2001. Localization of organic anion transporting polypeptide 4 (Oatp4) in rat liver and comparison of its substrate specificity with Oatp1, Oatp2 and Oatp3. *Pflugers Arch.* **443:** 188–195.

38. Cattori, V., B. Hagenbuch, N. Hagenbuch, B. Stieger, R. Ha, K. E. Winterhalter, and P. J. Meier. 2000. Identification of organic anion transporting polypeptide 4 (Oatp4) as a major full-length isoform of the liver-specific transporter-1 (rlst-1) in rat liver. *FEBS Lett.* **474:** 242–245.

39. Meng, L. J., P. Wang, A. W. Wolkoff, R. B. Kim, R. G. Tirona, A. F. Hofmann, and K. S. Pang. 2002. Transport of the sulfated, amidated

bile acid, sulfolithocholyltaurine, into rat hepatocytes is mediated by Oatp1 and Oatp2. *Hepatology.* **35:** 1031–1040.

40. Tobin, K. A., H. H. Steineger, S. Alberti, O. Spydevold, J. Auwerx, J. A. Gustafsson, and H. I. Nebb. 2000. Cross-talk between fatty acid and cholesterol metabolism mediated by liver X receptor-alpha. *Mol. Endocrinol.* **14:** 741–752.

41. Patel, D. D., B. L. Knight, A. K. Soutar, G. F. Gibbons, and D. P. Wade. 2000. The effect of peroxisome-proliferator-activated receptor-alpha on the activity of the cholesterol 7 alpha-hydroxylase gene. *Biochem. J.* **351:** 747–753.

42. Marrapodi, M., and J. Y. Chiang. 2000. Peroxisome proliferator-activated receptor alpha (PPARalpha) and agonist inhibit cholesterol 7alpha-hydroxylase gene (CYP7A1) transcription. *J. Lipid Res.* **41:** 514–520.

43. Kok, T., V. W. Bloks, H. Wolters, R. Havinga, P. L. Jansen, B. Staels, and F. Kuipers. 2003. Peroxisome proliferator-activated receptor alpha (PPARalpha)-mediated regulation of multidrug resistance 2 (Mdr2) expression and function in mice. *Biochem. J.* **369:** 539–547.

44. Hossain, M. A., M. Tsujita, F. J. Gonzalez, and S. Yokoyama. 2008. Effects of fibrate drugs on expression of ABCA1 and HDL biogenesis in hepatocytes. *J. Cardiovasc. Pharmacol.* **51:** 258–266.

45. Chinetti, G., S. Lestavel, V. Bocher, A. T. Remaley, B. Neve, I. P. Torra, E. Teissier, A. Minnich, M. Jaye, N. Duverger, et al. 2001. PPAR-alpha and PPAR-gamma activators induce cholesterol removal from human macrophage foam cells through stimulation of the ABCA1 pathway. *Nat. Med.* **7:** 53–58.

46. Rakhshandehroo, M., L. M. Sanderson, M. Matilainen, R. Stienstra, C. Carlberg, P. J. de Groot, M. Muller, and S. Kersten. 2007. Comprehensive analysis of PPARalpha-dependent regulation of hepatic lipid metabolism by expression profiling. *PPAR Res.* **2007:** 26839.

47. Rakhshandehroo, M., B. Knoch, M. Muller, and S. Kersten. 2010. Peroxisome proliferator-activated receptor alpha target genes. *PPAR Res.* **61:** 393–416.

48. Miyata, M., A. Tozawa, H. Otsuka, T. Nakamura, K. Nagata, F. J. Gonzalez, and Y. Yamazoe. 2005. Role of farnesoid X receptor in the enhancement of canalicular bile acid output and excretion of unconjugated bile acids: a mechanism for protection against cholic acid-induced liver toxicity. *J. Pharmacol. Exp. Ther.* **312:** 759–766.

49. Wang, R., P. Lam, L. Liu, D. Forrest, I. M. Yousef, D. Mignault, M. J. Phillips, and V. Ling. 2003. Severe cholestasis induced by cholic acid feeding in knockout mice of sister of P-glycoprotein. *Hepatology.* **38:** 1489–1499.

50. Wang, L., Y. K. Lee, D. Bundman, Y. Han, S. Thevananther, C. S. Kim, S. S. Chua, P. Wei, R. A. Heyman, M. Karin, et al. 2002. Redundant pathways for negative feedback regulation of bile acid production. *Dev. Cell.* **2:** 721–731.